

Fractal spectrum in twisted bilayer optical lattice

Xu-Tao Wan,¹ Chao Gao,^{2,3,*} and Zhe-Yu Shi^{1,†}

¹State Key Laboratory of Precision Spectroscopy,
East China Normal University, Shanghai 200062, China

²Department of Physics, Zhejiang Normal University, Jinhua, 321004, China

³Key Laboratory of Optical Information Detection and Display Technology of Zhejiang,
Zhejiang Normal University, Jinhua, 321004, China

(Dated: April 15, 2024)

The translation symmetry of a lattice is greatly modified when subjected to a perpendicular magnetic field [Zak, Phys. Rev. **134**, A1602 (1964)]. This change in symmetry can lead to magnetic unit cells that are substantially larger than the original ones. Similarly, the translation properties of a double-layered lattice alters drastically while two monolayers are relatively twisted by a small angle, resulting in large-scale moiré unit cells. Intrigued by the resemblance, we calculate the complete band structures of a twisted bilayer optical lattice and show that the geometric moiré effect can induce fractal band structures. The fractals are controlled by the twist angle between two monolayers and are closely connected to the celebrated butterfly spectrum of two-dimensional Bloch electrons in a magnetic field [Hofstadter, Phys. Rev. B **14**, 2239 (1976)]. We demonstrate this by proving that the twisted bilayer optical lattice can be mapped to a generalized Hofstadter's model with long-range hopping. Furthermore, we provide numerical evidence on the infinite recursive structures of the spectrum and give an algorithm for computing these structures.

In his seminal work on two-dimensional Bloch electrons in magnetic fields, Hofstadter discovers that the spectrum of the electrons constitutes a fractal graph. He demonstrated that the graph exhibits recursive self-similar structures which leads to “a very striking pattern somewhat resembling a butterfly” [1]. The pattern, now known as Hofstadter's butterfly, keeps fascinating both physicists and mathematicians. Numerous theoretical achievements have since been made to help to comprehend its self-similarity [2–4], fractal structure [5, 6], band topology [7–9] and wavefunction localization [10–12].

On the experimental side, considerable effort has also been devoted to reproducing Hofstadter's butterfly in various physical systems [13–21]. Most of these systems differ from Hofstadter's original work, which considers tight-binding Bloch electrons on a square lattice. Yet they all involve subdividing the energy bands of a lattice into minibands through enlarging the (magnetic) unit cell via an external magnetic field.

In this work, we study the band structures of the recently realized twisted bilayer optical lattice (TBOL) in cold atomic gases [22]. Intriguingly, we discover a hidden connection between the algebraic structures of the TBOL and Hofstadter's model. Inspired by this connection, we calculate the band structure of a TBOL and show that the spectrum is a butterfly-like fractal. It is worth emphasizing that the fractal spectrum is solely induced by the geometric moiré effect of the TBOL and does not require any time reversal breaking external field. The behavior of the fractal graph is determined by the twist angle of the TBOL rather than the magnetic flux. We further demonstrate that the TBOLs in the so-called imbalanced limit can be exactly mapped to Hofstadter's original model plus a long-range hopping term, providing

insights into the origin of the butterfly-like spectrum.

Models.—We consider a model of particles moving in a twisted double-layer of square lattices, which has been realized in atomic gases recently [22]. The system can be described by the following Hamiltonian,

$$H = \begin{pmatrix} \frac{\mathbf{p}^2}{2m_0} + V_1 - \frac{\delta}{2} & \Omega \\ \Omega & \frac{\mathbf{p}^2}{2m_0} + V_2 + \frac{\delta}{2} \end{pmatrix}. \quad (1)$$

Here, the two layers are simulated by the two spin components of the atoms (denoted by states 1 and 2). They are coupled through a microwave field with strength Ω and detuning δ . $V_1(x, y) = -\frac{V_0}{2}(\cos(2\pi x) + \cos(2\pi y))$ is the potential of a fixed square lattice, while V_2 is twisted around the origin by an angle θ , such that $V_2(x, y) = V_1(x \cos \theta + y \sin \theta, -x \sin \theta + y \cos \theta)$. For simplicity, we have assumed that the axis of the twist goes through the origin and the lattice spacing of both optical lattice is unity. The physical properties of the TBOL are determined by four energy scales, the lattice depth V_0 , the coupling strength Ω , the detuning δ , and the recoil energy of the optical lattice $E_r \equiv \frac{\hbar^2 \pi^2}{2m_0}$. In this work, we always consider the tight-binding limit, assumed by the condition $V_0 \gg E_r$.

Commensurate condition.—The TBOL described by Eq. (1) seems noticeably different from Hofstadter's model of charged particles in an external field. However, a deep connection can be revealed by a close inspection of the commensurate conditions for both models.

For Hofstadter's model, the magnetic field would modify the translation symmetry of the system, resulting in the so-called magnetic translation group [23, 24]. Consequently, the periodicity of the lattice relies on the rationality of the magnetic flux through a unit cell. Assuming that the magnetic flux is $\alpha\Phi$, where $\Phi \equiv \frac{h}{2e}$ is the mag-

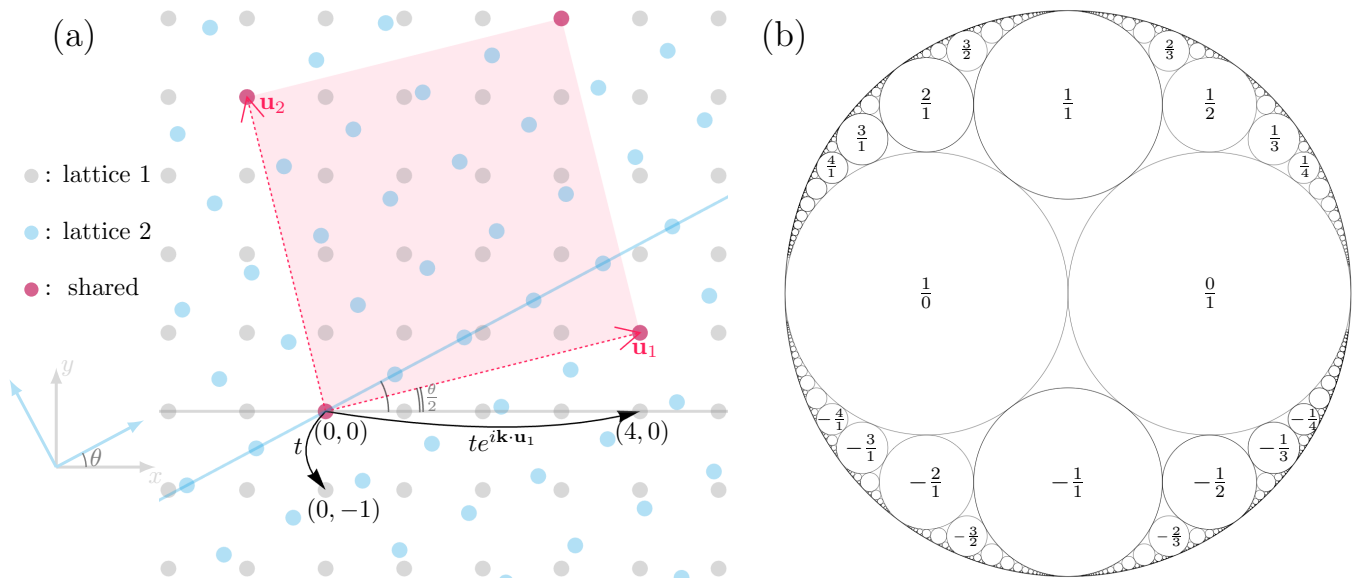


FIG. 1. (a) Moiré lattice created through twisting two square optical lattices. The twist angle is $\theta = \arccos \frac{15}{17}$ corresponding to $(p, q) = (1, 4)$. The unit vectors of the lattice are $\mathbf{u}_1 = (4, 1)$ and $\mathbf{u}_2 = (-1, 4)$. The unit cell is marked by the pink square with an area of $c = p^2 + q^2 = 17$. (b) The Apollonian gasket related to the commensurate condition described by Eq. (2). Each inner small circle represents a commensurate twist angle for the twisted bilayer square lattice. Each fraction at the center is the corresponding $\frac{p}{q}$.

netic flux quantum, the system is periodic if and only if the dimensionless parameter α is a rational number. If one writes $\alpha = p/q$, where p, q are coprime positive integers, each magnetic unit cell contains exactly q sites. Therefore, the band structure at this magnetic field consists of q bands, which suggests that the spectrum is a fractal because the denominator q is highly fluctuating while varying the magnetic field.

In comparison, the twist of a double-layered optical lattice also alters the overall translation structure of the TBOL, which leads to interference patterns known as the moiré patterns. The periodicity and the moiré unit cell of the lattice thus are determined by the relative twist angle θ between the two monolayers [25]. It can be shown that the TBOL forms a commensurate moiré lattice if and only if both $\cos \theta = a/c$ and $\sin \theta = b/c$ are rationals, i.e. θ is one of the acute angles of a Pythagorean triangle with integral side lengths a, b and c [26, 27]. Euclid proved that all primitive Pythagorean triples (a, b, c) may be expressed by two coprime integers p, q as $a = q^2 - p^2$, $b = 2pq$, $c = p^2 + q^2$. Using this formula, we obtain

$$\cos \theta = \frac{a}{c} = \frac{q^2 - p^2}{p^2 + q^2}, \quad \sin \theta = \frac{b}{c} = \frac{2pq}{p^2 + q^2}. \quad (2)$$

Similar to Hofstadter's model, we see that the geometric structure of a commensurate TBOL is determined by two integers p and q as well. As illustrated in Fig. 1, the unit vectors of the moiré lattice can be chosen as $\mathbf{u}_1 = (q, p)$ and $\mathbf{u}_2 = (-p, q)$ [28]. The area of a moiré unit cell is thus c times of the original unit cell of the square lattice.

We note that the commensurate condition of the TBOL already hints that there exists a hidden fractal structure in the moiré pattern of a TBOL. The hidden fractal is known as the Apollonian gasket or Apollonian net that is plotted in Fig. 1(b). To construct this pattern from Eq. (2), one can first plot a unit circle on the complex plane. This circle forms the largest circle of the Apollonian gasket, and it represents all the possible twists between two monolayers, as each point $e^{i\theta}$ on the circle represents a twist with angle θ . At every commensurate twist angle labeled by the integer pair (p, q) , one can plot a circle tangent to the unit circle from the inside with curvature $c + 1$, and the resulting diagram is then the Apollonian gasket shown in Fig. 1(b).

The Apollonian gasket is mathematically closely related to certain Diophantine equations and dynamic systems on hyperbolic manifolds [29, 30]. In this work, we will not discuss its mathematical importance, but list a few facts that help us understand the fractal band structures of a moiré lattice. First, the Apollonian gasket is a fractal with Hausdorff dimension around 1.3057 [31]. Since the curvature of each circle is $c + 1$, this indicates that the area of the moiré unit cell is also a highly fluctuating function of the twist angle θ . Second, the underlying algebra of the Hofstadter's butterfly is related to a fractal diagram known as the Ford circles [4]. Mathematically the Ford circles can be viewed as a special type of Apollonian gasket in the sense that they can be transformed into each other via a Möbius transformation [32]. From these two facts, it is clear that there may exist

some hidden connection between the geometric moiré effect and Hofstadter's model.

Imbalanced limit of TBOLs.—In the following section, we consider the imbalanced limit ($\delta \gg V_0, \Omega$) of a TBOL, and confirm this conjecture by demonstrating that the Hamiltonian (1) can be mapped to a generalized Hofstadter's model with long-range hopping.

In the imbalanced limit, one can treat V_2 as a perturbation, since the atoms in state 2 are far detuned. By adiabatically eliminating the high-energy state 2 and applying the tight-binding approximation, the low-energy physics of the TBOL can be described by the following effective lattice Hamiltonian [32]

$$H_I = -t \sum_{m,n} \left(a_{m+1,n}^\dagger a_{m,n} + a_{m,n+1}^\dagger a_{m,n} + h.c. \right) - \sum_{m,n} V_{m,n} a_{m,n}^\dagger a_{m,n} \quad (3)$$

with $V_{m,n} = v \cos[2\pi(m \cos \theta + n \sin \theta)] + v \cos[2\pi(m \sin \theta - n \cos \theta)]$. Here, $m, n \in \mathbb{Z}$ represent the x and y coordinates of a site, $a_{m,n}^\dagger$ ($a_{m,n}$) stands for the creation (annihilation) operator for the lowest band Wannier function of state 1 centered at (m, n) . The tunneling coefficient t and on-site potential strength v are related to the parameters in the original model by $t = \frac{4}{\sqrt{\pi}} E_r^{1/4} V_0^{3/4} \exp\left(-2\sqrt{\frac{V_0}{E_r}}\right)$ and $v = \Omega^2 V_0 / \delta^2$.

We note that H_I has been considered previously in Ref. [33, 34], in which it is pointed out that H_I may be viewed as an extension of the self-dual Aubry-André model [11] to a higher dimension. The focus of these works is primarily on the localization properties of the system for specific twist angles, while our work investigates the entire spectrum landscape for a wide range of twist angles. On the other hand, because of the time-reversal symmetry of the original model (1), the adiabatic elimination will not introduce any gauge field in the low-energy sector of the Hilbert space. Thus, the first Chern number of the TBOL bands must also vanish. This feature is distinct from other models such as twisted two-dimensional transition metal dichalcogenides [35, 36], where a pseudo magnetic field might emerge in the adiabatic limit [37].

To establish a connection between H_I and Hofstadter's model requires two steps. The first step is to map H_I to a one-dimensional lattice with long-range hopping by dimension reduction. Then one can use dimension extension to remap the model to a two-dimensional one that describes lattice particles moving in an external perpendicular magnetic field.

Dimension reduction.—We consider the TBOL with a twist angle θ determined by an integer pair (p, q) . To reduce H_I to a one-dimensional model, we utilize the periodicity of the lattice in one direction.

For example, consider the twist angle corresponding to $(p, q) = (1, 4)$ as illustrated in Fig. 1. The periods of

this TBOL are integral linear combinations of two unit vectors $\mathbf{u}_1 = (4, 1)$ and $\mathbf{u}_2 = (-1, 4)$. Exploiting the periodicity along the \mathbf{u}_1 direction, we may choose the unit cell as the chain of all the sites on the x -axis. By Bloch's theorem, the eigenfunctions of H_I can be written as the product of a plane wave along the \mathbf{u}_1 direction and a periodic function concerning the translation in \mathbf{u}_1 . Consequently, the Bloch Hamiltonian $H_{\mathbf{k}}$ becomes a one-dimensional model defined on the chain.

The dimension reduction introduces long-range hoppings into the Bloch Hamiltonian. To see this, note that the vertical hopping terms $a_{m,n+1}^\dagger a_{m,n} + h.c.$ in H_I describe couplings between different unit cells. These terms need to be converted into intra-unit-cell ones with the help of Bloch's theorem. For example, we may consider the inter-unit-cell hopping from the site $(0, 0)$ to $(0, -1)$ as shown in Fig. 1. By Bloch's theorem, the wavefunction at site $(0, -1)$ equals the wavefunction at site $(4, 0)$ multiplied by a phase factor $e^{-i\mathbf{k}\cdot\mathbf{u}_1}$, where \mathbf{k} is the (two-dimensional) crystal momentum. This inter-unit-cell hopping can thus be transformed into an intra-unit-cell one with hopping distance $d = 4$ and phase $\kappa = \mathbf{k}\cdot\mathbf{u}_1$.

The above analysis can be generalized to generic commensurate twist angles. The Bloch Hamiltonian $H_{\mathbf{k}}$ thus can be written as [32]

$$H_{\mathbf{k}} = -t \sum_m \left[a_{m+1}^\dagger(\mathbf{k}) a_m(\mathbf{k}) + e^{i\kappa} a_{m+d}^\dagger(\mathbf{k}) a_m(\mathbf{k}) + h.c. \right] - \sum_m v \left[\cos(2\pi m \cos \theta) + \cos(2\pi m \sin \theta) \right] a_m^\dagger(\mathbf{k}) a_m(\mathbf{k}). \quad (4)$$

Here, the hopping distance d satisfies the following congruence equation

$$p \cdot d \equiv q \pmod{c}. \quad (5)$$

The phase κ is given by $\kappa = \mathbf{k} \cdot \mathbf{R}$ with $\mathbf{R} = (d, 1)$. $a_m^\dagger(\mathbf{k}) = A^{-1/4} \sum_{n \in \mathbb{Z}} e^{in\mathbf{k}\cdot\mathbf{R}} a_{m+nd,n}^\dagger$ is the creation operator for a plane wave along the \mathbf{R} direction and A is the area of the system.

Dimension extension.—The arithmetic properties of the hopping distance d are vital for the dimension extension mapping. Here, we list the three most crucial properties, the proof of which can be found in the supplementary material [32]. I. Eq. (5) has a unique solution up to modulo c . Thus one can always find a hopping distance d such that $0 < d < c$. II. For large c , the hopping distance is approximately proportional to \sqrt{c} in general. III. The following congruence relation holds $d \cdot (q^2 - p^2) \equiv -2pq \pmod{c}$, which, along with Eq. (2), implies that

$$e^{i2\pi m d \cos \theta} = e^{-i2\pi m \sin \theta}. \quad (6)$$

We can now utilize the dimension extension method [38, 39] to remap $H_{\mathbf{k}}$ to a two-dimensional

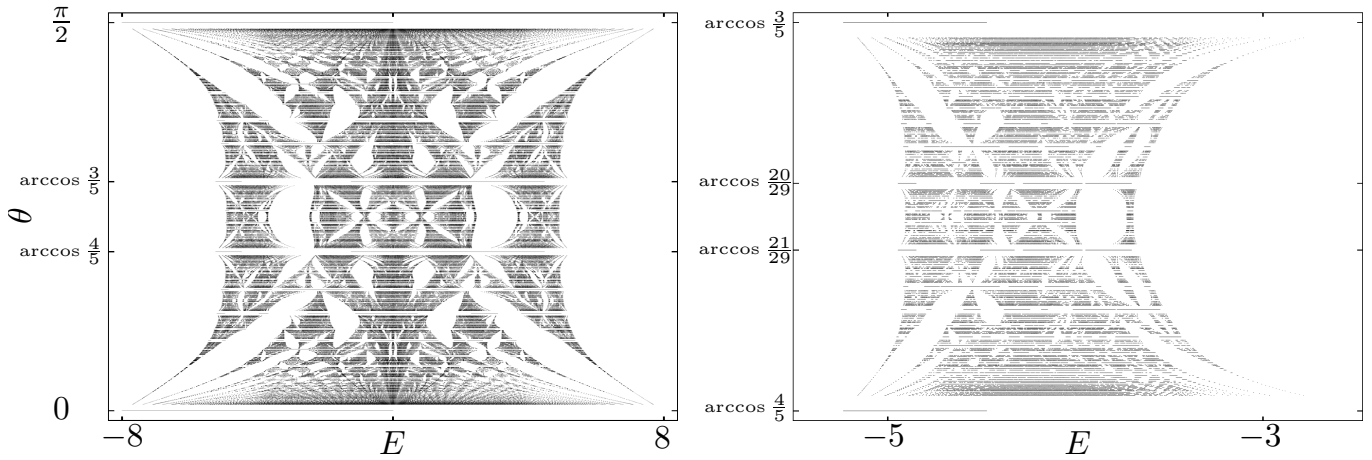


FIG. 2. Left: Tight-binding energy spectrum of the TBOL in the imbalanced limit, H_I , calculated with $v/2 = t = 1$. The graph exhausts all commensurate twist angles corresponding to (p, q) with $q \leq 40$. Right: A self-similar subgraph of the left, which contains the low-energy part of the spectrum with twist angles between $\theta^u = \arccos \frac{3}{5}$ and $\theta^l = \arccos \frac{4}{5}$ and $q \leq 55$.

model. This is achieved by treating the on-site potential terms of $H_{\mathbf{k}}$ as the kinetic energies originating from hoppings along a fictitious y' -direction perpendicular to the x -axis. Therefore, we may write the two on-site potential terms in $H_{\mathbf{k}}$ as the kinetic energies of the following hoppings (with $k_{y'} = 0$),

$$\begin{aligned} \cos(2\pi m \cos \theta) &\rightarrow \sum_{n'} (e^{i2\pi m \cos \theta} |m, n' + 1\rangle \langle m, n'| + h.c.), \\ \cos(2\pi m \sin \theta) &\rightarrow \sum_{n'} (e^{i2\pi m d \cos \theta} |m, n' + d\rangle \langle m, n'| + h.c.), \end{aligned}$$

where $|m, n'\rangle$ stands for the wavefunction at site $x = m$, $y' = n'$, and we have used the crucial property Eq. (6) in the second line.

As a result, we reach the following two-dimensional Hamiltonian,

$$\begin{aligned} H_{2D} = & - \sum_{m, n'} (t|m + 1, n'\rangle \langle m, n'| + te^{i\kappa}|m + d, n'\rangle \langle m, n'| \\ & + ve^{i2\pi m \cos \theta}|m, n' + 1\rangle \langle m, n'| \\ & + ve^{i2\pi m d \cos \theta}|m, n' + d\rangle \langle m, n'| + h.c.). \end{aligned} \quad (7)$$

Note that m -dependent phases of the hoppings in y' -direction exactly correspond to the phases induced by a magnetic field under the Landau gauge [1]. H_{2D} thus describes a square lattice model in a θ -controlled magnetic field with both the nearest-neighbor and long-range hoppings [40].

Symmetries and self-similarities of the spectrum.—We calculate and plot the spectrum of H_I at different commensurate twist angles in Fig. 2. As anticipated, we obtain a butterfly-like graph with intricate fractal structures.

The graph demonstrates certain (approximate) symmetries of the spectrum of H_I . First, it exhibits a reflection symmetry about the horizontal line $\theta = \pi/4$, which

is a consequence of the reflection symmetry of the underlying square lattice. Second, the entire graph appears to have an *approximate* reflection symmetry about the vertical line $E = 0$. This can be understood by applying a gauge transformation $a_m(\mathbf{k}) \rightarrow (-1)^m a_m(\mathbf{k})$ to H_{1D} . The transformation flips the sign of the kinetic energy terms but does not affect the on-site potentials. The spectrum for commensurate θ thus does not possess an exact $E \rightarrow -E$ symmetry. However, for almost all of the incommensurate twist angles, $\cos \theta$ and $\sin \theta$ are both irrational. In these cases, one may find a translation on m that induces phase changes close enough to π in both on-site potentials of H_{1D} . The spectrum thus exhibits the $E \rightarrow -E$ symmetry for almost all twist angles, resulting in a graph with an approximate vertical reflection symmetry.

One also observes recursive self-similar substructures in Fig. 2. For example, we plot a self-similar subgraph of the whole spectrum between twist angles $\theta_1^u = \arccos \frac{3}{5}$ and $\theta_1^l = \arccos \frac{4}{5}$. These angles correspond to integer pairs $(p_1^u, q_1^u) = (1, 2)$ and $(p_1^l, q_1^l) = (1, 3)$. Moreover, in Fig. 2, one can observe another self-similar subgraph between $\theta_2^u = \arccos \frac{20}{29}$ and $\theta_2^l = \arccos \frac{21}{29}$, which correspond to $(p_2^u, q_2^u) = (3, 7)$ and $(p_2^l, q_2^l) = (2, 5)$. We conjecture that this self-similar sequence continues infinitely and the corresponding angles satisfy the recursive relation [32]

$$\frac{p_{n+1}^{u,l}}{q_{n+1}^{u,l}} = \frac{1 + p_n^{u,l}/q_n^{u,l}}{3 + p_n^{u,l}/q_n^{u,l}} \quad (8)$$

with $(p_0^u, q_0^u) = (1, 1)$ and $(p_0^l, q_0^l) = (0, 1)$. Note that

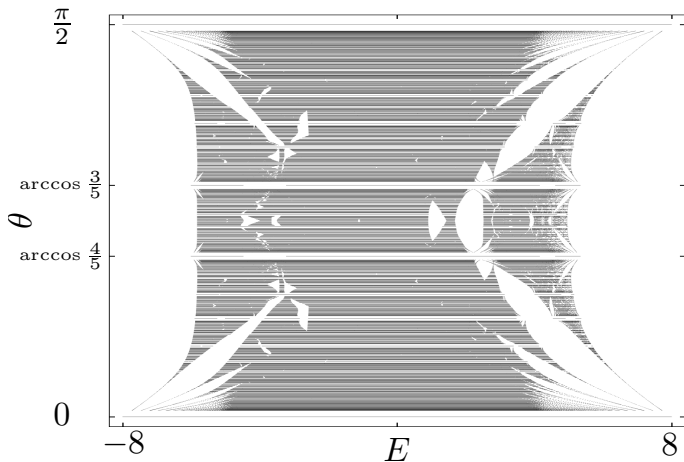


FIG. 3. Tight-binding energy spectrum of the TBOL in the balanced limited calculated with $\delta = 0$, $V_0 = 10E_r$, $\Omega = 4t$, and $t = 1$. The graph exhausts all commensurate twist angles corresponding to (p, q) with $q \leq 40$.

both p_n^u/q_n^u and p_n^l/q_n^l have the same limit

$$\lim_{n \rightarrow \infty} \frac{p_n^{u,l}}{q_n^{u,l}} = \frac{1}{1 + \frac{2}{1 + \frac{1}{1 + \frac{2}{1 + \dots}}}} = \sqrt{2} - 1 = \tan \frac{\pi}{8}, \quad (9)$$

which indicates θ_n^u and θ_n^l are infinitely close to the line $\theta = \pi/4$ in the $n \rightarrow +\infty$ limit according to Eq. (2).

The mapping between the imbalanced Hamiltonian H_I and the lattice model with magnetic fields H_{2D} cannot be directly generalized to TBOLs with small detuning $\delta \lesssim V_0, \Omega$. However, since the commensurate condition remains valid, one may still expect the spectrum to be a fractal graph that resembles Fig. 2. In Fig. 3, we plot the spectrum of the TBOL in the balanced limit $\delta = 0$ [32], which indeed appears to be fractal as expected. In comparison with Fig. 2, one can see that the approximate reflection symmetry about the vertical line is broken in the balanced limit. Furthermore, a self-similar subgraph in the high-energy part of the spectrum between $\theta_1^u = \arccos \frac{3}{5}$ and $\theta_1^l = \arccos \frac{4}{5}$ can be observed, while it is difficult to separate a self-similar subgraph in the low-energy part because of band overlapping.

Conclusions & remarks.—In summary, we show that the geometric moiré effect of TBOL can lead to a fractal spectrum that is related to Hofstadter’s butterfly. These results may be experimentally tested by measuring the single-particle density of states in TBOLs using radio-frequency or Bragg spectroscopy. It is worth noting that, unlike the moiré unit cell which we have shown to be highly fluctuating, the moiré pattern of a twisted bilayer system actually changes smoothly while twisting the lat-

tice. The fact suggests that the *low-energy* physics of a moiré system is indeed continuous with respect to the twist angle. While this continuous *low-energy* physics can be observed in our calculations such as the low-energy Landau levels presented in Fig. 2 and also be theoretically described by specific models such as the famous continuous model for twisted bilayer graphenes [41], this work represents an initial exploration of the entire spectrum landscape of two-dimensional moiré lattices. For future investigations, we believe it would be valuable to study the origins of the self-similar substructures, band topologies, and transport properties of TBOL and other twisted bilayer systems.

We are grateful for the helpful discussions with Ce Wang and Hui Zhai. This work is supported by the Natural Science Foundation of Zhejiang Province, China (Grant Nos. LR22A040001, LY21A040004), and the National Natural Science Foundation of China (Grant No. 12074342).

* gaochao@zjnu.edu.cn

† zyshi@lps.ecnu.edu.cn

- [1] D. R. Hofstadter, *Energy levels and wave functions of Bloch electrons in rational and irrational magnetic fields*, *Physical Review B* **14**, 2239 (1976).
- [2] G. Wannier, *A result not dependent on rationality for Bloch electrons in a magnetic field*, *Physica Status Solidi* **88**, 757 (1978).
- [3] M. Wilkinson, *An exact renormalisation group for Bloch electrons in a magnetic field*, *Journal of Physics A: Mathematical and General* **20**, 4337 (1987).
- [4] I. I. Satija, *The Butterfly in the Quantum World: The story of the most fascinating quantum fractal* (Morgan & Claypool Publishers, 2016).
- [5] Y. Last and B. Simon, *Eigenfunctions, transfer matrices, and absolutely continuous spectrum of one-dimensional Schrödinger operators*, *Inventiones Mathematicae* **135**, 329 (1999).
- [6] A. Avila and S. Jitomirskaya, *The Ten Martini Problem*, *Annals of Mathematics* **170**, 303–342 (2009).
- [7] D. J. Thouless, M. Kohmoto, M. P. Nightingale, and M. den Nijs, *Quantized Hall conductance in a two-dimensional periodic potential*, *Physical Review Letters* **49**, 405 (1982).
- [8] P. Streda, *Theory of quantised Hall conductivity in two dimensions*, *Journal of Physics C: Solid State Physics* **15**, L717 (1982).
- [9] M.-C. Chang and Q. Niu, *Berry phase, hyperorbits, and the Hofstadter spectrum*, *Physical Review Letters* **75**, 1348 (1995).
- [10] D. J. Thouless, *Electrons in disordered systems and the theory of localization*, *Physics Reports* **13**, 93 (1974).
- [11] S. Aubry and G. André, *Analyticity breaking and Anderson localization in incommensurate lattices*, *Ann. Israel Phys. Soc* **3**, 18 (1980).
- [12] S. Y. Jitomirskaya, *Metal-insulator transition for the almost Mathieu operator*, *Annals of Mathematics* **150**, 1159 (1999).

- [13] U. Kuhl and H.-J. Stöckmann, *Microwave realization of the Hofstadter butterfly*, *Physical Review Letters* **80**, 3232 (1998).
- [14] C. Albrecht, J. Smet, K. Von Klitzing, D. Weiss, V. Umansky, and H. Schweizer, *Evidence of Hofstadter's fractal energy spectrum in the quantized Hall conductance*, *Physical Review Letters* **86**, 147 (2001).
- [15] M. Aidelsburger, M. Atala, M. Lohse, J. T. Barreiro, B. Paredes, and I. Bloch, *Realization of the Hofstadter Hamiltonian with ultracold atoms in optical lattices*, *Physical Review Letters* **111**, 185301 (2013).
- [16] H. Miyake, G. A. Siviloglou, C. J. Kennedy, W. C. Burton, and W. Ketterle, *Realizing the Harper Hamiltonian with laser-assisted tunneling in optical lattices*, *Physical Review Letters* **111**, 185302 (2013).
- [17] C. R. Dean, L. Wang, P. Maher, C. Forsythe, F. Ghahari, Y. Gao, J. Katoch, M. Ishigami, P. Moon, M. Koshino, T. Taniguchi, K. Watanabe, K. L. Shepard, J. Hone, and P. Kim, *Hofstadter's butterfly and the fractal quantum Hall effect in moiré superlattices*, *Nature* **497**, 598 (2013).
- [18] L. A. Ponomarenko, R. V. Gorbachev, G. L. Yu, D. C. Elias, R. Jalil, A. A. Patel, A. Mishchenko, A. S. Mayorov, C. R. Woods, J. R. Wallbank, M. Mucha-Kruczynski, B. A. Piot, M. Potemski, I. V. Grigorieva, K. S. Novoselov, F. Guinea, V. I. Fal'ko, and A. K. Geim, *Cloning of Dirac fermions in graphene superlattices*, *Nature* **497**, 594 (2013).
- [19] B. Hunt, J. D. Sanchez-Yamagishi, A. F. Young, M. Yankowitz, B. J. LeRoy, K. Watanabe, T. Taniguchi, P. Moon, M. Koshino, P. Jarillo-Herrero, and R. C. Ashoori, *Massive Dirac Fermions and Hofstadter Butterfly in a van der Waals Heterostructure*, *Science*, *Science* **340**, 1427 (2013).
- [20] P. Roushan, C. Neill, J. Tangpanitanon, V. M. Bastidas, A. Megrant, R. Barends, Y. Chen, Z. Chen, B. Chiaro, A. Dunsworth, A. Fowler, B. Foxen, M. Giustina, E. Jeffrey, J. Kelly, E. Lucero, J. Mutus, M. Neeley, C. Quintana, D. Sank, A. Vainsencher, J. Wenner, T. White, H. Neven, D. G. Angelakis, and J. Martinis, *Spectroscopic signatures of localization with interacting photons in superconducting qubits*, *Science* **358**, 1175 (2017).
- [21] X. Lu, B. Lian, G. Chaudhary, B. A. Piot, G. Romagnoli, K. Watanabe, T. Taniguchi, M. Poggio, A. H. MacDonald, B. A. Bernevig, *et al.*, *Multiple flat bands and topological Hofstadter butterfly in twisted bilayer graphene close to the second magic angle*, *Proceedings of the National Academy of Sciences* **118**, e2100006118 (2021).
- [22] *Atomic Bose-Einstein condensate in twisted-bilayer optical lattices*, *Nature* **615**, 231 (2023).
- [23] J. Zak, *Magnetic translation group*, *Physical Review* **134**, A1602 (1964).
- [24] J. Zak, *Magnetic translation group. II. Irreducible representations*, *Physical Review* **134**, A1607 (1964).
- [25] Without loss of generality, we assume $\theta \in [0, \frac{\pi}{2})$ in this paper.
- [26] C. Huang, F. Ye, X. Chen, Y. V. Kartashov, V. V. Konotop, and L. Torner, *Localization-delocalization wavepacket transition in Pythagorean aperiodic potentials*, *Scientific Reports* **6**, 32546 (2016).
- [27] P. Wang, Y. Zheng, X. Chen, C. Huang, Y. V. Kartashov, L. Torner, V. V. Konotop, and F. Ye, *Localization and delocalization of light in photonic moiré lattices*, *Nature* **577**, 42 (2020).
- [28] In the following, we shall focus on commensurate TBOLs where p and q have opposite parity. This is because if both p and q are odd, we may consider another pair p', q' , with $p' = \frac{q+p}{2}$ and $q' = \frac{q-p}{2}$. One may show that p', q' are coprime integers with opposite parity. The twist angle θ' defined by (p', q') is related to the original twist angle θ by $\theta' = \theta + \frac{\pi}{2}$. The TBOL corresponding to the odd-odd integer pair (p, q) can thus be converted into the opposite-parity (p', q') case.
- [29] D. Mumford, C. Series, D. J. Wright, and D. Wright, *Indra's pearls: The vision of Felix Klein* (Cambridge University Press, 2002).
- [30] R. L. Graham, J. C. Lagarias, C. L. Mallows, A. R. Wilks, and C. H. Yan, *Apollonian circle packings: number theory*, *Journal of Number Theory* **100**, 1 (2003).
- [31] C. T. McMullen, *Hausdorff dimension and conformal dynamics, III: Computation of dimension*, *American Journal of Mathematics* **120**, 691 (1998).
- [32] See supplementary material for details.
- [33] T. Devakul and D. A. Huse, *Anderson localization transitions with and without random potentials*, *Physical Review B* **96**, 214201 (2017).
- [34] A. Szabó and U. Schneider, *Mixed spectra and partially extended states in a two-dimensional quasiperiodic model*, *Physical Review B* **101**, 014205 (2020).
- [35] H. Yu, M. Chen, and W. Yao, *Giant magnetic field from moiré induced Berry phase in homobilayer semiconductors*, *National Science Review* **7**, 12 (2020).
- [36] D. Zhai and W. Yao, *Theory of tunable flux lattices in the homobilayer moiré of twisted and uniformly strained transition metal dichalcogenides*, *Physical Review Materials* **4**, 094002 (2020).
- [37] It is worth mentioning that the system considered in Ref. [35, 36] also possesses time reversal symmetry. However, if one focuses on electrons near the K point of the Brillouin zone, an effective Hamiltonian that breaks the time-reversal symmetry can be obtained. Therefore, a synthetic magnetic field might emerge after adiabatically eliminating one of the layers. This mechanism is intriguing yet different from the one discussed in this work, as it introduces a constant magnetic flux through each moiré unit cell.
- [38] L.-J. Lang, X. Cai, and S. Chen, *Edge states and topological phases in one-dimensional optical superlattices*, *Physical Review Letters* **108**, 220401 (2012).
- [39] Y. E. Kraus, Y. Lahini, Z. Ringel, M. Verbin, and O. Zeitlinger, *Topological states and adiabatic pumping in quasicrystals*, *Physical Review Letters* **109**, 106402 (2012).
- [40] We note that the phases in the cosine functions in $H_{\mathbf{k}}$ play the role of the momentum along the fictitious y' -direction of the two-dimensional model. Thus only the Bloch states with $k_{y'} = 0$ of H_{2D} can be mapped to eigenstates of $H_{\mathbf{k}}$. Yet Bloch states with finite $k_{y'}$ are also valuable, as they correspond to eigenstates of TBOL with finite displacement between V_1 and V_2 .
- [41] R. Bistritzer and A. H. MacDonald, *Moiré bands in twisted double-layer graphene*, *Proceedings of the National Academy of Sciences* **108**, 12233 (2011).